Journal of
Applied Crystallography
ISSN 0021-8898

Received 23 March 2011
Accepted 19 May 2011

Enhancement in crystalline perfection and optical properties of benzophenone single crystals: the remarkable effect of a liquid crystal

S. K. Kushwaha,[a,b] N. Vijayan,[a] K. K. Maurya,[a] A. Kumar,[a] B. Kumar,[b] K. Somayajulu[c] and G. Bhagavannarayana[a]*

[a]X-ray Analysis Section, National Physical Laboratory, Dr K. S. Krishnan Marg, New Delhi, Delhi 110012, India, [b]Department of Physics and Astrophysics, University of Delhi, New Delhi, Delhi 110007, India, and [c]Department of Agricultural Chemistry, Indian Agricultural Research Institute, Pusa Campus, New Delhi, Delhi 110012, India. Correspondence e-mail: bhagavan@mail.nplindia.ernet.in

The remarkable enhancement of the crystalline perfection of benzophenone (BP) crystals induced by liquid crystal (LC) doping has been investigated, and has in turn led to better optical properties. High-resolution X-ray diffractometry demonstrates that the structural grain boundaries present in pure crystals can be eliminated when the crystal is grown with LC doping. Thus, the high alignment capability of LCs has for the first time been utilized to enhance the quality of BP bulk single crystals. The LC-doped crystal exhibits higher optical transparency over its entire transparent region. The optical polarizing behaviour of the doped BP crystal is also improved.

© 2011 International Union of Crystallography
Printed in Singapore – all rights reserved

1. Introduction

Nonlinear optical (NLO) single crystals have a wide range of applications in areas such as high-energy lasers for inertial confinement fusion research, colour displays, electro-optic switches, frequency conversion *etc.* (Zaitseva & Carman, 2001; Badan *et al.*, 1993). Owing to their anisotropic nature, structural defects like point defects, dislocations and grain boundaries reduce or completely mask the useful physical properties of single crystals. Therefore, to realize the full efficiency of devices based on single crystals, the crystals must be free from such defects (Bhagavannarayana, Ananthamurthy *et al.*, 2005; Bhagavannarayana, Budakoti *et al.*, 2005). The physical properties of single crystals can be modified for tailor-made applications by adding suitable dopants and functional groups (Sweta & Tanusree, 2007; Bhagavannarayana *et al.*, 2008). However, such dopants and functional groups do not control defects in crystals. Rather, if their concentration is above a critical limit they may reduce crystalline perfection and hence impair the physical properties (Kushwaha *et al.*, 2010; Bhagavannarayana, Budakoti *et al.*, 2005; Bhagavannarayana & Kushwaha, 2010). However, there are some special classes of dopants that may help to improve the molecular alignment of the crystals and modify the crystal quality. Liquid crystals (LCs) possess the ability to self-organize and can induce alignment in the structures surrounding them at the molecular level *via* electric field interaction, as reported for the aligning and reorientation of carbon nanotubes (Dierking *et al.*, 2004). This self-aligning behaviour of LCs may provide a driving force for better molecular arrangement at the solid–liquid interface during crystal growth. In the present investigation, for the first time to the best of our knowledge, we have exploited the alignment capability of LCs to improve the crystalline perfection of benzophenone (BP) bulk single crystals grown by the Czochralski (CZ) method. BP is a promising organic NLO material with a second-harmonic generation (SHG) efficiency almost three times better than that of potassium dihydrogen phosphate (KDP). It crystallizes in an orthorhombic structure in space group $P2_12_12_1$ (Lammers *et al.*, 2000). Bulk single crystals of BP are prone to inherent structural defects like dislocations, grain boundaries *etc.* (Sankaranarayanan & Ramasamy, 2005; Masaru *et al.*, 1992; Bleay *et al.*, 1978). Different dopants in BP have been studied (Arivanandhan *et al.*, 2006; Sixl *et al.*, 1986) for the modification of various physical properties, but no literature is available regarding the analysis of crystalline perfection and its correlation with modified physical properties. We have grown single crystals of pure and LC-doped BP and analysed their crystal structures by single-crystal X-ray diffraction. NMR spectroscopy was performed to investigate the incorporation of LCs into the BP crystal lattice. High-resolution X-ray diffractometry (HRXRD) was carried out to assess the influence of LCs on crystalline perfection. Optical transmission spectra were recorded in the entire UV–vis–NIR range of wavelengths and photoluminescence (PL) spectroscopy was employed to assess the defects in the crystals. Birefringence was examined using an optical polarizing microscope. The remarkable observed enhancement in the crystalline perfection and optical properties of BP crystals by LC doping is discussed in detail.

2. Experimental

2.1. Crystal growth

Single crystals of BP were grown by the Czochralski (CZ) technique. For this, a CZ crystal puller designed, developed

and fabricated at the Indian National Physical Laboratory (NPL) (Bhagavannarayana *et al.*, 2011) was used. BP and the SCE-13 liquid crystal were procured from CDH, India, and BDH, UK, respectively. The SCE-13 liquid crystal falls into the category of ferroelectric liquid crystals and above room temperature it exhibits three phase transitions: $SmC^* \rightarrow SmA^*$ at 334 K, $SmA^* \rightarrow N$ at 359 K and $N \rightarrow I$ at 376 K (Kao *et al.*, 1977), where Sm, N and I stand for smectic, nematic and isotropic, respectively. LC molecules in the smectic phase show a degree of translational order (http://plc.cwru.edu/tutorial/enhanced/files/lc/phase/phase.htm). Owing to the ordering nature of the smectic phase at and below the growth temperature used here (323 K), SCE-13 was expected to induce molecular ordering for BP molecules during the crystal growth process. The LC (0.02 wt%) was mixed thoroughly with BP powder and then melted. The melted charge was kept at 338 K for 4 h for full homogeneous mixing. The temperature of the charge was lowered slowly and crystals were grown at 323 K, just 1 K above the melting point of BP (322 K; Vijayan *et al.*, 2006), which was found to be the optimum value for growth. The pulling and rotational rates were set at 3 mm h^{-1} and 30 r min^{-1}, respectively. The temperature of the furnace was controlled using a Eurotherm temperature controller with an accuracy of ±0.1 K. For bulk crystal growth, seed crystals were prepared from the pure crystal, which was grown primarily using the microcapillary method (Hiscocks, 1969). The growth conditions for both crystals were kept identical and the harvested pure and LC-doped crystals are shown in Figs. 1(*a*) and 1(*b*), respectively. Compared with the pure crystal, the LC-doped crystal is apparently more transparent. The yellow arrows at the top of each crystal indicate the growth direction, *i.e.* [100]. Specimens from the bulk crystals were cut normal to [100]. Cut and polished specimens were subjected to crystalline perfection and other optical characterization.

2.2. Nuclear magnetic resonance spectroscopy

To investigate the incorporation of LC molecules in the grown BP single crystals, ^1H and ^{13}C NMR spectra were recorded using a Bruker Avance III NMR spectrometer controlled by *Topspin* software (Bruker AXS Inc., Madison, Wisconsin, USA). Dimethylsulfoxide was used as solvent and spectrometer was operated at 400 MHz.

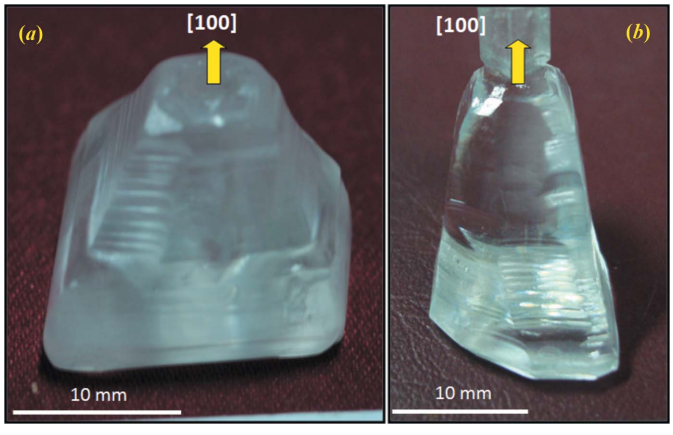

Figure 1
Photographs of (*a*) pure and (*b*) LC-doped BP single crystals. The yellow arrows indicate the growth direction of the crystals, which is [100].

2.3. High-resolution multicrystal X-ray diffractometry

The crystalline perfection of the pure and doped crystals was evaluated by employing HRXRD. A multicrystal X-ray diffractometer developed at the NPL (Lal & Bhagavannarayana, 1989) was used to record high-resolution rocking curves. A fine-focus (0.4 × 8 mm) X-ray source energized by a well stabilized 2 kW Philips X-ray generator (PW 1743) was employed. The well collimated and monochromated Mo $K\alpha_1$ beam obtained from the three monochromator Si crystals set in a dispersive (+,−,−) configuration was used as the incident X-ray beam (Lal & Bhagavannarayana, 1989; Bhagavannarayana & Kushwaha, 2010). This arrangement improves the spectroscopic purity ($\Delta\lambda/\lambda << 10^{-5}$) of the incident beam. The divergence of the incident beam in the horizontal plane (plane of diffraction) was estimated to be << 3″. The specimen crystal is aligned in the (+,−,−,+) configuration. Owing to the dispersive configuration, even though the lattice constants of the monochromator crystal(s) and the specimen are different, the unwanted dispersion broadening in the diffraction curve of the specimen crystal is insignificant (Bhagavannarayana & Kushwaha, 2010). The specimen can be rotated about a vertical axis, which is perpendicular to the plane of diffraction, with a minimum angular interval of 0.4″. The diffracted intensity is measured using a scintillation counter. The rocking curves were recorded by varying the glancing angle (the angle between the incident X-ray beam and the surface of the specimen) around the Bragg diffraction peak position θ_B (taking zero as the reference point), starting from a suitable arbitrary glancing angle θ. The detector was kept at the same angular position of $2\theta_B$ with a wide opening for its slit, the so-called ω scan, as explained in our recent article (Bhagavannarayana & Kushwaha, 2010). In the present study, the X-ray power, the size of the beam and the configuration of the diffractometer were kept the same for both specimens throughout the experiments. The physical surfaces of the crystals corresponding to the (200) diffraction plane were suitably lapped and polished, and the diffraction curves of these planes were recorded in symmetrical Bragg geometry.

2.4. Photoluminescence spectroscopy

The PL excitation and emission spectra for the pure and doped specimens were recorded on a Perkin–Elmer LS-55 spectrophotometer at room temperature. A 395 nm filter was placed between the specimen and the detector to prevent the harmonics of the excitation wavelength from reaching the detector. The surfaces of the crystals were well lapped and polished before being subjected to the measurements.

2.5. UV–vis–NIR spectroscopy

The transmission spectra from [100]-cut 2 mm-thick crystals were recorded over the entire UV–vis–NIR range of wave-

lengths (200–1100 nm) on a Perkin–Elmer Lambda 35 spectrometer. The incident beam was directed so as to fall normally on the surface of the crystals.

2.6. Polarized optical microscopy

The optical polarizing nature of the grown crystals was analysed using an optically polarized microscope. The specimens were mounted on a rotational table and the beam transmitted through the crystal was converted into an electrical signal, which was measured by an oscilloscope with the crystal rotated through 360° around the axis along the incident beam. A digital camera was used to record photographs at the maximum and minimum conditions of polarization. All experimental settings were kept identical for both crystals.

3. Results and discussion

3.1. NMR analysis

NMR spectroscopy is a powerful tool to reveal the number and nature of hydrogen and carbon atoms present in organic compounds (Dani, 1995). The technique is helpful in assessing the overall molecular structure of a compound and is also useful for investigating variations in the electronic structure of crystals (Sharma, 2000). The ^{1}H and ^{13}C NMR spectra recorded for pure and LC-doped specimens of BP are shown in Fig. 2. Both kinds of spectra have identical features for both pure and doped specimens. The pure BP molecule consists of two symmetrical benzene rings connected through a carbonyl group (C═O), as shown in the insets of the figures. In the ^{1}H NMR spectra, three signals are observed which correspond to the ^{1}H present in BP: 2H (triplet; *t*) at δ = 7.50 p.p.m., 1H (*t*) at δ = 7.62 p.p.m. and 2H (doublet) at δ = 7.69 p.p.m. In the ^{13}C NMR spectra, the signal at δ = 196.0 p.p.m. corresponds to the carbonyl group (C═O) attached to the two symmetrical benzene rings. However, the four signals in the δ range between 128 and 138 p.p.m. correspond to the four distinct C atoms in the benzene rings (one attached to the carbonyl group, and the other three corresponding to the *ortho*, *meta* and *para* positions). The ^{1}H and ^{13}C NMR spectra for the LC-doped BP specimen do not show any chemical shift or any extra peak compared with the pure BP specimen. Therefore, the NMR results reveal that the doped BP crystals do not contain dopant LC molecules.

3.2. High-resolution XRD analysis

Single-crystal X-ray diffraction analysis was carried out to investigate the crystal structure and unit-cell parameters of the BP specimens. However, no variations in the crystal system or lattice parameters of the pure and doped BP crystals were observed. These results confirm that the LC molecules were not incorporated into the BP crystal lattice during the growth of the single crystals, in agreement with the NMR analysis. The unit-cell parameters of BP (a = 9.11, b = 10.566 and c = 8.855 Å) are much smaller than the LC molecules (~20–30 Å in length; http://liq-xtal.cwru.edu/lcdemo.htm) and therefore exclude the possibility of incorporating LC molecules into the BP lattice matrix. However, LC molecules present in the molten BP during the growth process may lead to modifications in crystalline perfection, as revealed by HRXRD. Fig. 3(*a*) shows the rocking curve (RC) for a typical CZ-grown undoped BP single-crystal specimen using the (200) diffracting

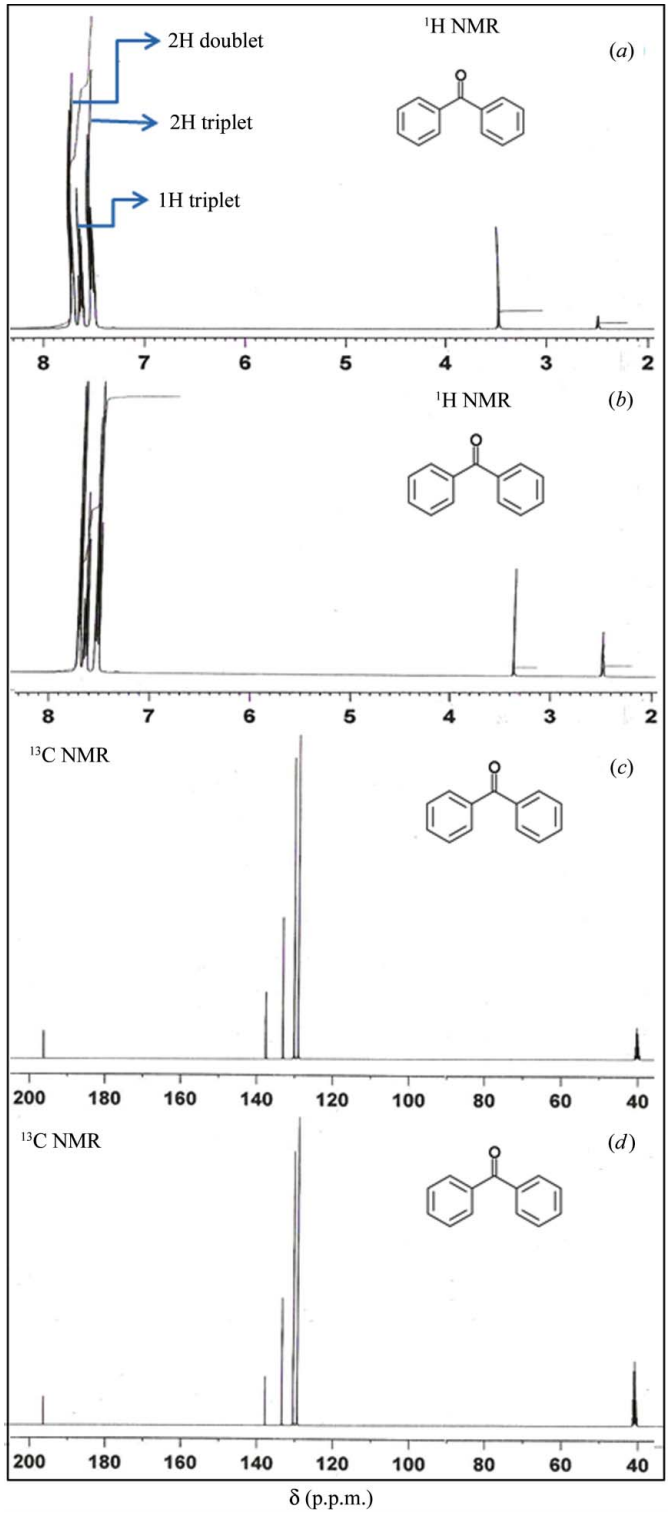

Figure 2
The ^{1}H NMR spectra for (*a*) pure and (*b*) LC-doped BP specimens, and the ^{13}C NMR spectra for (*c*) pure and (*d*) LC-doped BP specimens.

plane in symmetrical Bragg geometry. The solid line (convoluted curve) is well fitted to the experimental points (filled circles). On deconvolution of the diffraction curve, it is clear that the curve contains three additional peaks, two of them 45 and 88″ away from the main peak on the higher-angle side and the third one 66″ away from the main peak on the lower-angle side. These three additional peaks correspond to three internal structural low- (tilt angle > 1′ but less than a degree) and very low angle (tilt angle ≤ 1′) boundaries (Bhagavannarayana, Ananthamurthy *et al.*, 2005). The tilt angles (defined as the misorientation angle between the two crystalline regions on both sides of the structural grain boundary) of these grain boundaries are 45, 43 and 66″ from their adjoining regions. The FWHMs of the different boundaries are 32, 52, 31 and 100″, as shown in Fig. 3(*a*). Although the specimen contains grain boundaries, the low FWHM values and the low angular spread of the diffraction curve of around 400″ (less than one-tenth of a degree) indicate that the crystalline perfection is reasonably good. It may be mentioned that the observation of such very low angle boundaries is possible because of the high resolution of the multicrystal X-ray diffractometer used in the present investigation. The low-angle boundaries in the pure BP crystals may be formed as a result of thermal fluctuations at the liquid–solid interface, as the fractional change in temperature $\Delta T/T$ is supposed to be high at its low melting point (~322 K).

It is well known that LCs have a great tendency for alignment below their solid–liquid phase transition temperature, as a result of their large electric dipole moment (Dierking *et al.*, 2004). This unique aligning nature is presumed to assist the improvement in crystalline perfection of BP single crystals grown in the presence of LCs. The RC for an LC-doped BP single crystal shown in Fig. 3(*b*) was recorded under identical conditions to that of Fig. 3(*a*) for pure BP. The single sharp peak shows that the crystal does not contain any structural grain boundaries. The FWHM of the diffraction curve is 25″, which is close to that expected from the plane-wave dynamic theory of X-ray diffraction for a perfect single crystal (Batterman & Cole, 1964). Details of the theoretical aspects of diffraction curves and how they can be obtained from dynamic theory are described in our recent articles (Bhagavannarayana & Kushwaha, 2010; Senthil Kumar *et al.*, 2011). For a better comparison of crystals with considerable differences in quality, as in the present case of undoped and doped BP crystals, one should discuss the integrated intensity ρ, *i.e.* the total area under the diffraction curve, which differs tremendously between the diffraction curves of the doped and undoped specimens. To understand this aspect, the following theoretical background is essential.

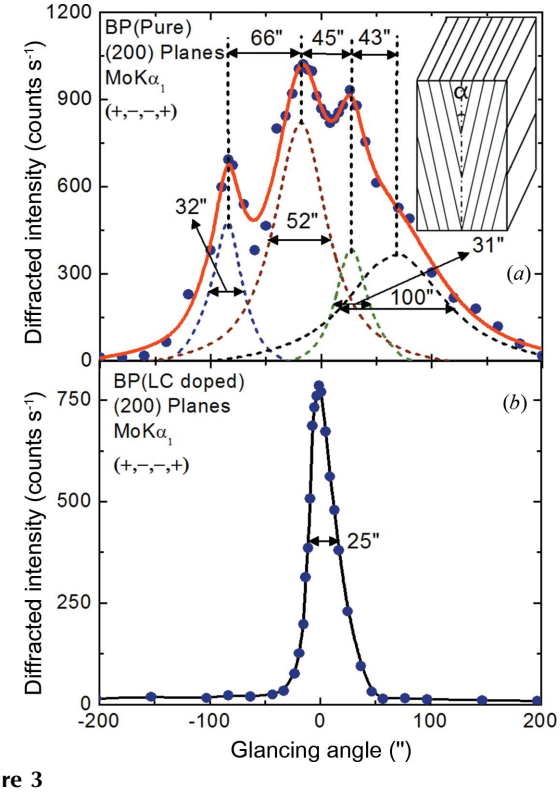

Figure 3
High-resolution X-ray diffraction rocking curves for the (200) diffraction planes of (*a*) pure and (*b*) LC-doped BP single crystals. The inset indicates a schematic for a structural grain boundary.

There are two main theories that enable the calculation of the intensity of X-ray diffraction from single crystals, namely the kinematic theory and the dynamic theory. In a crystal structure, the atoms are arranged in a periodic fashion. The smallest building block is the unit cell. In the kinematic theory, each unit cell acts as an independent unit for the purpose of X-ray diffraction, and the intensity of the diffracted beam is obtained by adding up the contribution of all such cells. The interaction of diffracted waves from different unit cells is ignored. The amplitude and phase of the resultant wave are defined by the structure factor F_{hkl} for the *hkl* reflection (it may also be denoted $F_{\rm H}$), and the intensity of the scattered X-ray I is proportional to $|F_{hkl}|^2$ or

$$I \propto |F_{hkl}|^2 \quad \text{where} \quad F_{hkl} = \sum_j f_j \exp[-2\pi i(hu_j + kv_j + lw_j)], \tag{1}$$

where u_j, v_j and w_j are the fractional coordinates of the atom whose scattering factor is f_j and the summation is over all the atoms in the unit cell. The structure factor can be zero for a set of lattice planes. Finite intensity will be expected only from those sets of lattice planes for which $F_{hkl} \neq 0$. The kinematic theory has been very successful in structural crystallography. For quantitative intensity analysis it is necessary to use small specimens. Corrections due to primary and secondary extinctions are necessary. One is mainly concerned with the determination of the integrated intensity, which is basically the area under the diffraction curve as mentioned above. For an ideally imperfect (or mosaic) crystal with a linear absorption coefficent μ, it can be expressed as (James, 1950; *International Tables for X-ray Crystallography*, 1962)

$$\rho_{\rm mosaic} = \frac{N^2\lambda^3}{2\mu}|F_{hkl}|^2\left(\frac{e^2}{mc^2}\right)^2\frac{1+|\cos 2\theta|^2}{2\sin 2\theta}, \tag{2}$$

where N is the number of unit cells, θ is the Bragg diffraction angle and e/mc^2 is the classical electron radius = 2.818×10^{-15} m (e and m are the charge and mass of the electron, respectively, and c is the speed of light). The incident beam is assumed to be unpolarized.

In the case of large perfect crystals, the kinematic approach cannot be used to give peak intensities or the shapes of diffraction curves. The dynamic theory of X-ray diffraction (James, 1950; Batterman & Cole, 1964; Pinsker, 1978) takes into account interactions between waves scattered from all irradiated atoms or scattering units. Any atom inside the crystal receives scattered waves from all the other atoms, in addition to the incident beam (after attenuation due to scattering and absorption). In this approach, the integrated intensity for an ideally perfect crystal is given by (James, 1950; *International Tables for X-ray Crystallography*, 1962)

$$\rho_{\rm perfect} = \frac{8}{3\pi} N\lambda^2 |F_{hkl}| \left(\frac{e^2}{mc^2}\right) \frac{1+|\cos 2\theta|}{2\sin 2\theta}. \qquad (3)$$

One important difference between equations (2) and (3) is that in the case of ideally mosaic crystals the integrated intensity is proportional to the square of the structure factor, whereas in ideally perfect crystals it is simply proportional to the magnitude of the structure factor. Because of this clear contrast, the experimental value of $\rho_{\rm mosaic}$ is expected to be greater than that of $\rho_{\rm perfect}$. Therefore, as observed in the present case, one can conclude that the quality of the LC-doped crystal is much superior.

The above discussion and the low FWHM of the rocking curve in Fig. 3(*b*) reveal that the crystal is not only free of boundaries but also free of mosaic blocks. The present results show that LC molecules strongly influence the perfection of BP crystals and avoid the formation of structural grain boundaries. The large molecular size of LCs provides a suitable means of attaining a high level of molecular alignment in bulk crystals without their incorporation into the lattice of the host crystal.

3.3. PL emission analysis

Defects in single crystals play an important role in the assessment of their optical properties and PL is very sensitive to the presents of such defects (Yue *et al.*, 1999; Tournie *et al.*, 1996). The PL excitation and emission spectra for both pure and LC-doped BP single crystals were recorded under identical conditions and are shown in Fig. 4. The excitation spectra of both crystals indicate a strong absorption at 311 nm and the emission spectra were recorded corresponding to this excitation wavelength. The pure BP crystal exhibits a high optical density for excitation and a high intensity for PL emission at 447 nm. The strong blue emission from the pure BP crystal is attributed to intrinsic defects, which act as colour centres (Pankratov *et al.*, 2007; Xu *et al.*, 1998). This is in agreement with the above HRXRD analysis. In our earlier studies we also observed the dependence of the PL intensity on the intrinsic crystal defects in LiF crystals (Bhagavannarayana *et al.*, 2011). For the LC-doped crystals in the present work, the defects are significantly reduced and the emission intensity is drastically reduced almost by half. However, neither a shift in the peak position nor any additional peak was observed as a result of doping. As is clear from the NMR analysis, the LC molecules are not incorporated into the crystal lattice, but only provide a driving force (catalytic action) to the BP molecules for better alignment, owing to their large dipole moment and highly aligning nature (Dierking *et al.*, 2004).

3.4. UV–vis–NIR analysis

The optical transmission spectra in the entire UV–vis–NIR range for pure and doped BP crystals are shown in Fig. 5. Both

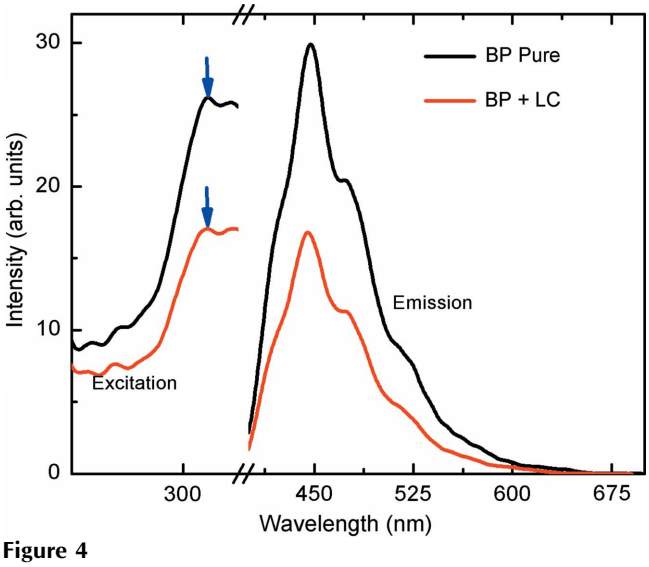

Figure 4
The photoluminescence excitation and emission spectra. The solid black line indicates data for the pure BP crystal and the solid red line data for the LC-doped BP crystal.

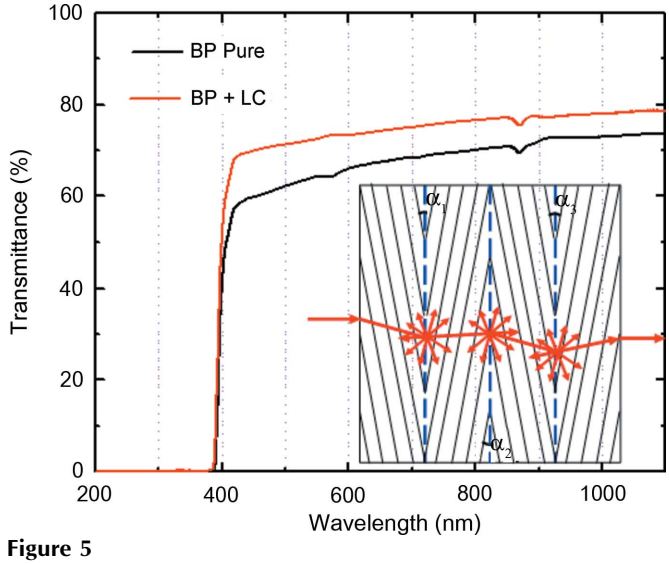

Figure 5
The UV–vis–NIR transmission spectra of pure (solid black line) and LC-doped BP (solid red line) single crystals. The inset indicates multiple refraction and scattering of the incident beam at the grain boundaries persisting in pure BP crystals.

crystals have good optical transparency over the whole wavelength range of 400–1100 nm, but the doped crystal is the better of the two. This enhancement in the optical transparency of the doped crystal may be attributed to the absence of structural grain boundaries, since grain boundaries in a specimen lead to multiple refraction and scattering of the incident beam and hence reduce the optical transparency (Apetz & van Bruggen, 2003; Schroeder & Rosolowski, 1981). Because of the different misorientations of the grain boundaries in the pure crystal, changes occur in the direction of the incident beam. To visualize this concept a schematic is shown as an inset to Fig. 5.

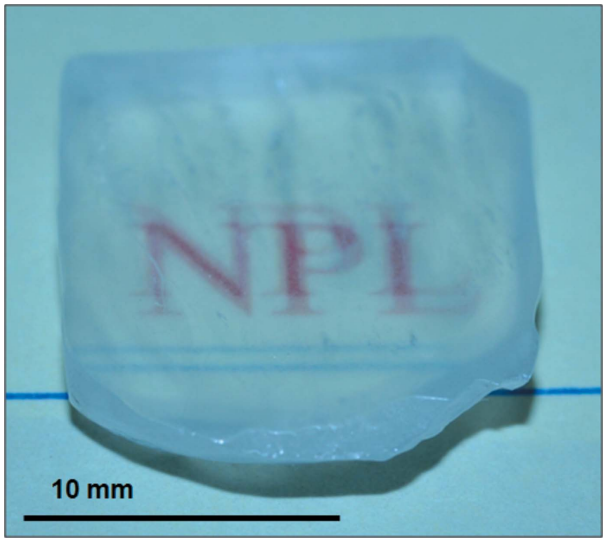

Figure 6
Cut and polished BP single crystal, showing its birefringent behaviour.

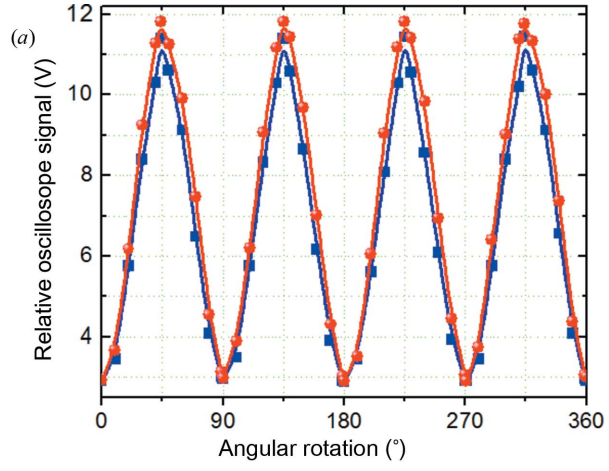

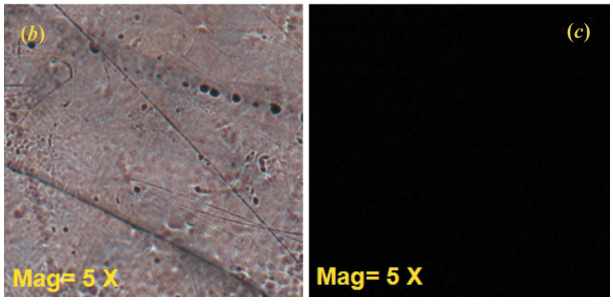

Figure 7
(*a*) Graphs indicating the optical polarization behaviour of pure (red solid line and points) and LC-doped (blue solid line and points) crystals. (*b*) and (*c*) show photographs of the bright and dark stages recorded at the maxima and minima of the transmission, respectively.

3.5. Birefringence analysis

BP is a birefringent material and therefore has the ability to polarize an optical electromagnetic beam. In Fig. 6 one can clearly see two images of the letters 'NPL' and of a straight line behind a single crystal of BP. These two images are due to splitting of the incident beam into ordinary (n_o) and extraordinary (n_e) components. Plots of the measured oscilloscope signal *versus* angular rotation for the doped and undoped crystals are shown in Fig. 7(*a*). As the crystals were rotated from 0 to 360°, four maxima and four minima were observed, corresponding to bright and dark states, respectively. The four maxima correspond to bright states occurring due to splitting of the beam into ordinary and extraordinary components (Flossmann *et al.*, 2005; Harris *et al.*, 1964). Both pure and doped crystals show the same behaviour with angular rotation. However, compared with the pure crystal, the LC-doped crystal exhibits a higher signal corresponding to the bright states, whereas no change is observed in the minima of the plots, corresponding to the dark states. This increase in the signal for the doped crystal at the bright states may be attributed to the enhanced optical transparency. Photographs taken of the bright and dark states are shown in Figs. 7(*b*) and 7(*c*), respectively. There is only a nominal increase in the optical signal due to polarization, for the following reason. Optical polarizability is a direction-dependent property and hence different grains in the crystal make different angles with the incident light. Therefore, in a crystal containing structural grain boundaries, the expected optical polarizability is less than that of a perfect crystal of the same material. However, as observed experimentally, the structural grains are misoriented to each other by an average angle (tilt angle) of around an arcminute. Optical polarizability is not very sensitive to such small angles, which could be why there is only a slight difference between the optical polarizability of pure and LC-doped BP.

4. Conclusions

We have successfully exploited the high ordering/aligning capability of LCs to grow nearly perfect bulk single crystals of BP by the CZ technique. Structural grain boundaries, which commonly persist in pure BP single crystals, have successfully been eliminated. We also conclude that LCs with a large electric dipole moment lead to a significant enhancement in crystalline perfection and optical properties. The enhanced crystalline perfection and optical properties suggest the suitability of BP crystals for high-energy laser photonic applications. Our present finding may be extended to other low-melting organic NLO crystals to improve their physical properties.

The authors thank Professor R. C. Budhani, Director, NPL, for continuous encouragement in carrying out this work under the in-house (CSIR) project No. OLP-070332. We express our gratitude to Dr A. M. Biradar, Dr D. Haranath and Dr N. Bahadur for useful discussions. SKK acknowledges the CSIR for providing a Senior Research Fellowship under grant No. 31/1(293)/2008-EMR-I.

References

Apetz, R. & van Bruggen, M. P. B. (2003). *J. Am. Ceram. Soc.* **86**, 480–486.

Arivanandhan, M., Sanjeeviraja, C., Sankaranarayanan, K., Das, S. K., Samanta, G. K. & Datta, P. K. (2006). *Opt. Mater.* **28**, 324–330.

Badan, J., Hierle, R., Perigaud, A. & Zyss, J. (1993). *NLO properties of Organic Molecules and Polymeric Materials*, American Chemical Society Symposium Series, Vol. 233. Washington, DC: American Chemical Society.

Batterman, B. W. & Cole, H. (1964). *Rev. Mod. Phys.* **36**, 681–717.

Bhagavannarayana, G., Ananthamurthy, R. V., Budakoti, G. C., Kumar, B. & Bartwal, K. S. (2005). *J. Appl. Cryst.* **38**, 768–771.

Bhagavannarayana, G., Budakoti, G. C., Maurya, K. K. & Kumar, B. (2005). *J. Cryst. Growth*, **282**, 394–401.

Bhagavannarayana, G. & Kushwaha, S. K. (2010). *J. Appl. Cryst.* **43**, 154–162.

Bhagavannarayana, G., Kushwaha, S. K., Shakir, Mohd. & Maurya, K. K. (2011). *J. Appl. Cryst.* **44**, 122–128.

Bhagavannarayana, G., Parthiban, S. & Meenakshisundaram, S. (2008). *Cryst. Growth Des.* **8**, 446–451.

Bleay, J., Hooper, R. M., Narang, R. S. & Sherwood, J. N. (1978). *J. Cryst. Growth*, **43**, 589–596.

Dani, V. R. (1995). *Organic Spectroscopy*. New Delhi: Tata McGraw–Hill.

Dierking, I., Scalia, G., Morales, P. & LeClere, D. (2004). *Adv. Mater.* **16**, 865–869.

Flossmann, F., Schwarz, U. T., Maier, M. & Dennis, M. R. (2005). *Phys. Rev. Lett.* **95**, 253901.

Harris, S. E., Amman, E. O. & Chang, I. C. (1964). *J. Opt. Soc. Am.* **54**, 1267–1278.

Hiscocks, S. E. R. (1969). *J. Mater. Sci.* **4**, 310–312.

International Tables for X-ray Crystallography (1962). Vol. III, ch. 3, p. 195. Birmingham: Kynoch Press.

James, R. W. (1950). *The Optical Principles of the Diffraction of X-rays*. London: G. Bell and Sons.

Kao, O.-C., Lyuu, J.-F., Lin, H.-R. & Lee, J.-Y. (1977). *Mol. Cryst. Liq. Cryst.* **302**, 21–34.

Kushwaha, S. K., Shakir, Mohd., Maurya, K. K., Shah, A. L., Wahab, M. A. & Bhagavannarayana, G. (2010). *J. Appl. Phys.* **108**, 033506.

Lal, K. & Bhagavannarayana, G. (1989). *J. Appl. Cryst.* **22**, 209–215.

Lammers, D., Betzler, K., Xue, D. & Zhao, J. (2000). *Phys. Status Solidi A*, **180**, R5–R7.

Masaru, T., Shigeki, M., Akira, U., Qi, T. & Kenichi, K. (1992). *Jpn. J. Appl. Phys.* **31**, 2202–2205.

Pankratov, V., Grigorjeva, L., Millers, D. & Yochum, H. M. (2007). *Phys. Status Solidi. C*, **4**, 801–804.

Pinsker, Z. G. (1978). *Dynamical Scattering of X-rays in Crystals*. Berlin: Springer-Verlag.

Sankaranarayanan, K. & Ramasamy, P. (2005). *J. Cryst. Growth*, **280**, 467–473.

Schroeder, J. & Rosolowski, J. H. (1981). *Proc. SPIE Int. Soc. Opt. Eng. (USA)*, **297**, 156–168.

Senthil Kumar, K., Moorthy Babu, S. & Bhagavannarayana, G. (2011). *J. Appl. Cryst.* **44**, 313–318.

Sharma, Y. R. (2000). *Elementary Organic Spectroscopy*. New Delhi: S. Chand.

Sixl, H., Mathes, R., Schaupp, A., Ulrich, K. & Huber, R. (1986). *Chem. Phys.* **107**, 105–121.

Sweta, M. & Tanusree, K. (2007). *Opt. Mater.* **30**, 508–512.

Tournie, E., Morhain, C., Neu, G., Faurie, J. P., Triboulet, R. & Ndap, J. O. (1996). *Appl. Phys. Lett.* **68**, 1356–1358.

Vijayan, N., Bhagavannarayana, G., Ramesh Babu, R., Gopalakrishnan, R., Maurya, K. K. & Ramasamy, P. (2006). *Cryst. Growth Des.* **6**, 1542–1546.

Xu, S. J., Li, G., Chua, S. J., Wang, X. C. & Wang, W. (1998). *Appl. Phys. Lett.* **72**, 2451–2453.

Yue, G., Lorentzen, J. D., Lin, J., Han, D. & Wang, Q. (1999). *Appl. Phys. Lett.* **75**, 492–494.

Zaitseva, N. & Carman, L. (2001). *Prog. Cryst. Growth Charact.* **43**, 1–118.